

Article

The Influence of CBD Parameters on the Energy Gap of ZnS Narcissus-Like Nanostructured Thin Films

Mohammed Hussein Khalil, Raghad Y. Mohammed  and Mohammed Aziz Ibrahim * 

Department of Physics, College of Science, University of Duhok, Duhok 42001, Iraq; mohamadswary@uod.ac (M.H.K.); ssraghad@uod.ac (R.Y.M.)

* Correspondence: m_aziz7951@uod.ac; Tel.: +964-750-458-2358

Abstract: Recently, the efficient preparation techniques of zinc sulfide (ZnS) nanostructured films have drawn great attention due to their potential applications in optoelectronics. In this study, the low-cost and high-yield chemical bath deposition (CBD) technique was used to deposit ZnS nanostructured thin films. The effect of various deposition parameters such as time, pH, precursor concentration, and temperature on the morphology and energy bandgap (E_g) of the prepared thin films were investigated. The characterization of the prepared thin films revealed the formation of polycrystalline ZnS with Narcissus-like nanostructures. Moreover, the optical characterization showed inverse proportionality between both the transmission and E_g of the nanostructured thin films and the variation of the deposition parameters. A range of different E_g values between 3.92 eV with 20% transmission and 4.06 eV with 80% transmission was obtained. Tuning the E_g values and transmission of the prepared nanostructured films by manipulating the deposition parameters of such an efficient technique could lead to applications in optoelectronics such as solar cells and detectors.

Keywords: CBD; ZnS thin films; growth; energy bandgap; nanostructure



Citation: Khalil, M.H.; Mohammed, R.Y.; Ibrahim, M.A. The Influence of CBD Parameters on the Energy Gap of ZnS Narcissus-Like Nanostructured Thin Films. *Coatings* **2021**, *11*, 1131. <https://doi.org/10.3390/coatings11091131>

Academic Editors: Mircea Nasui and Angela De Bonis

Received: 28 July 2021

Accepted: 7 September 2021

Published: 17 September 2021

Publisher's Note: MDPI stays neutral with regard to jurisdictional claims in published maps and institutional affiliations.



Copyright: © 2021 by the authors. Licensee MDPI, Basel, Switzerland. This article is an open access article distributed under the terms and conditions of the Creative Commons Attribution (CC BY) license (<https://creativecommons.org/licenses/by/4.0/>).

1. Introduction

Zinc sulfide is one of the most important large bandgap II-VI semiconductors, which have recently been identified as some of the best optoelectronic computing materials because of their useful properties, in particular their nontoxicity [1]. ZnS is an essential semiconducting material with a large direct bandgap of about 3.6–4 eV in the bulk [2,3]. ZnS as a white powdered compound is also known as zinc blende or sphalerite [4]. As a hexagonal crystalline structure, it has both wurtzite and synthetic mineral. However, it can also exist in cubic structure, which is more stable in this form [5].

ZnS nanostructures have been successfully synthesized in different nanostructure types such as nanowires [6], nanobelts [6,7], quantum dots [8], and nanotubes [9]. They can be integrated into a wide range of nanoscale devices, in particular piezotronics, photovoltaics, and photodetectors [9–12]. In addition, ZnS has also been considered as the best material to be used as an alternative buffer layer for cadmium sulfide (CdS) in CZTS solar cells [13], light-emitting diodes [14], catalysis [15], gas sensors [16], thermal sensors [17], and biosensors [18].

ZnS thin films are prepared by several methods such as spray pyrolysis [19,20], molecular beam epitaxy [21], successive ionic layer adsorption and reaction technique [22], pulsed laser deposition [23], electrodeposition [24], and CBD [25–27]. The CBD technique is widely used due to its low cost, low deposition temperature, and easy coating of large surfaces. In the CBD technique, the consistency of the deposited film depends on the temperature, the deposition time, the reactant concentration, and the pH of the bath [28–30].

In this work, ZnS Narcissus-like nanostructured thin films were prepared using the CBD technique for a short period of only ten minutes. To the best of our knowledge, the formation of such nanostructures within this short period of time has not been reported yet. The E_g of the prepared films was well controlled depending on different deposition

parameters. As a result, diverse and wide E_g values were obtained and this could widen their application for optoelectronic devices.

2. Materials and Methods

Glass substrates with dimensions of ($25 \times 75 \times 1$ mm³) were used to deposit ZnS thin films. The substrates were soaked in chromic acid for 24 h, washed with distilled water, and rinsed in acetone. Then, they were ultrasonically cleaned with distilled water, dried, and then kept in a desiccator.

ZnS thin films were prepared using 80 mL of 0.2 M zinc acetate ($\text{Zn}(\text{CH}_3(\text{COO})_2$), 8 mL of 0.25 M ammonia (NH_4OH), and 160 mL of 0.2 M thiourea (Tu) ($\text{SC}(\text{NH}_2)_2$), using a chemical bath deposition technique in an alkaline solution. All chemical materials were bought from pro analysis ACS company without further purification. The solution was stirred with a magnetic stirrer, as illustrated in Figure S1, at room temperature. Different bath compositions were used to prepare solutions, as shown in Table S1. The substrates were then immersed in a beaker containing the reaction mixture. The beaker was placed in a water bath at a temperature of (80 ± 2 °C). Then, it was heated with continuous stirring to the required temperature of deposition. The pH was measured with pH meter type (Jenway3505). The substrates were then taken out after a suitable time. They were washed with distilled water and ultrasonic agitation to remove the porous zinc sulfide overlayer, then dried in hot air and evacuated in the desiccator.

The surface morphology and structural properties were characterized and studied using field-emission scanning electron microscopy (FESEM, ZEISS, Oberkochen, Germany) and analytical X- Pert PRO (MRD model) ($\text{Cu K}\alpha = 1.5406$ Å at 40 kV, 30 mA) in the 2θ range from (10° to 80°) with a scanning rate of $1^\circ/\text{min}$. The optical transmittance spectra were recorded by the UV-VIS Spectrophotometer (Jenway, Bibby Scientific Ltd, Stone, UK) in the range of 300–1100 nm. The E_g of the thin films is calculated from Tauc's equation, as shown below:

$$(\alpha \cdot hv)^2 = A (hv - E_g) \quad (1)$$

where α is the absorption coefficient that is given by ($\alpha = 2.303 \log (T/d)$), A is the absorption, hv is the incident photon energy, E_g , T is the transmittance, and d is the film thickness [31].

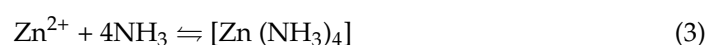
The thickness of the thin films was measured using the optical interferometer technique [32], in which thickness (d) is calculated by the following formula:

$$d = \frac{\lambda}{2} \cdot \frac{\Delta x}{x} \quad (2)$$

where λ is the wavelength of the He-Ne laser (632.8 nm), Δx is the distance between two fringes, and x is the fringe width.

3. Results and Discussion

Mass transport of reactants, adsorption, surface diffusion, reaction, nucleation, and growth are the fundamental aspects of the CBD growth mechanism. ZnS nanostructured films are formed by the decomposition of Tu ion source) in an alkaline solution containing zinc acetate (Zn^{2+} ion source) and (NH_4OH) as a complex agent. The deposition method is based on the slow release of Zn^{2+} and S^{2-} ions into the solution with the addition of NH_3 as a complex agent [33,34]. The process of the deposition can be illustrated depending on the following two reaction steps:



The yield complex then reacts with sulfide ions to form ZnS nanostructures as follows:



To accelerate the deposition process, the chemical bath was heated, and thus the chemical reaction rate of deposition was improved according to Ostwald's ripening process. At higher temperatures, the rate of reduction of sulfur increases, and the number of nucleation centers increases [34,35].

The investigation of ZnS thin films growth as a function of different deposition parameters is given in Figure 1.

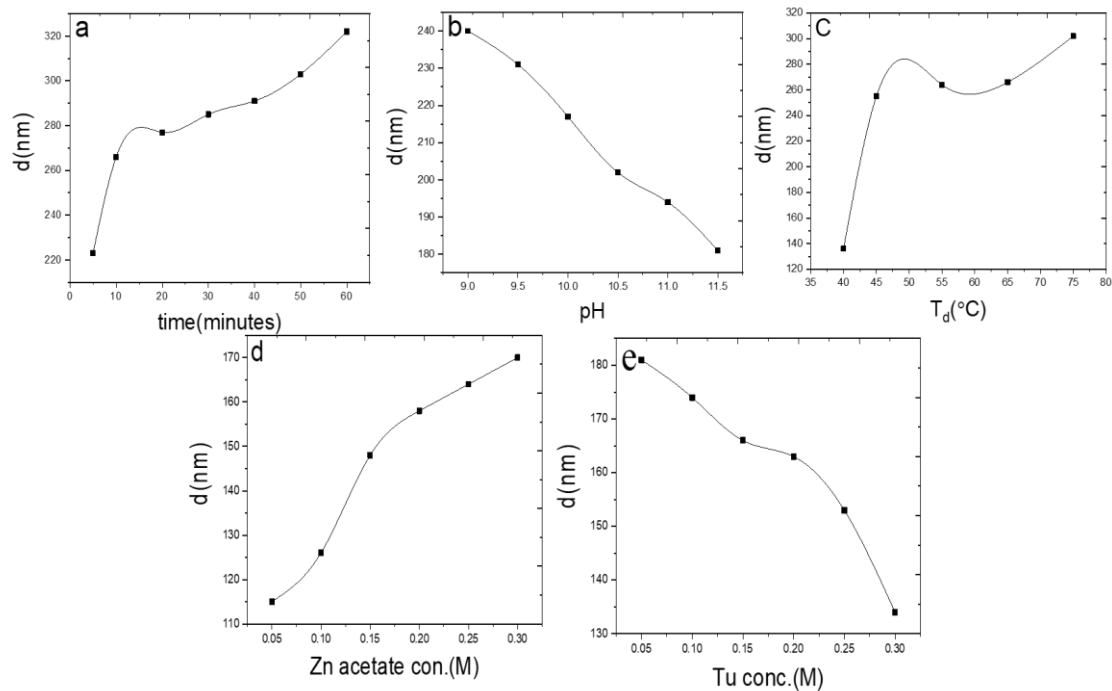


Figure 1. The thickness variation of ZnS thin film (where pH = 10, $t = 10$ min, $T = 65$ °C, zinc acetate and Tu-concentration concentration = 0.2 M) as a function of different, (a) deposition time (t_d), (b) pH, (c) deposition temperature (T_d), (d) zinc acetate concentration, and (e) Tu-concentration.

Figure 1a shows a significant increase in the thickness of the film of more than 260 nm after only ten minutes of the deposition time. Afterward, the growth of the film slightly increased without reaching the saturation limit. This is due to the increase of the rate of deposition [36,37]. A similar trend of the growth rate of the nanostructured films can also be seen in Figure 1c,d, at which the film's growth rate increases with the increase of both temperatures and Zn^{2+} concentration, respectively. Furthermore, Figure 1c shows a significant increase in the film thickness with a low temperature of only 45 °C. In this region, the rate of deposition is high due to high concentrations of Zn and S [36,38,39]. In contrast, the film thicknesses were decreased with the increase of both pH and Tu-concentration, as shown in Figure 1b,e. This is an indication of not having a sufficient amount of Zn^{2+} and S^{2-} ions released from Tu given the growth temperature range used in this study. It also implies that the growth of ZnS film requires a threshold concentration of precursor Tu to sustain the growth process [40]. The X-ray diffraction pattern of ZnS nanostructured thin films can be seen in Figure 2. It can be clearly found that the deposited films have a hexagonal structure with four peaks at $2\theta = 31.87^\circ$, 34.44° , 36.36° , and 56.68° . These peaks of ZnS films correspond to the (104), (106), (1010), and (203) planes of the wurtzite hexagonal ZnS phase according to the standard JCPDS data (01-072-0162) (01-072-0163) (01-079-2204) (01-080-0007). Different reports on CBD-ZnS films have shown the formation of the other phases into the films rather than the above patterns. These mixed phases can produce different effects on films, which sometimes are not easy to identify and control. Thus, the repeatability of the reported method is another challenge to obtaining ZnS films with high quality for the CBD technique [41].

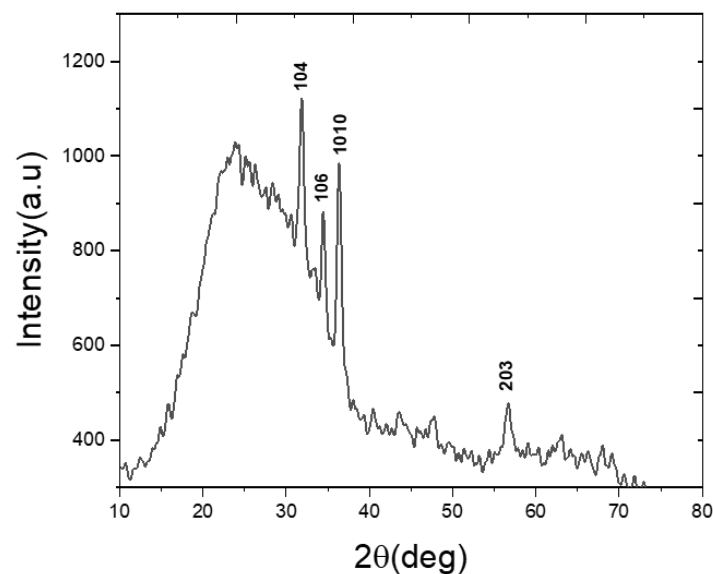


Figure 2. X-ray diffraction patterns of ZnS Narcissus-Like nanostructured thin films. Prepared at $T_d = 65\text{ }^\circ\text{C}$ pH = 10, $t = 10$ min. Zn conc. = 0.2 M, Tu-conc. = 0.2 M.

A small variation in pH had a significant effect on the morphology of the ZnS nanostructured thin films. When the solution pH was fixed at nine, cone-like (leaf) shapes appeared (Figure 3a). After increasing the pH of the solution to 10, the flower-like structures started to form, as shown in Figure 3b. After increasing the pH to 10.5, the Narcissus-Like nanostructures were formed Figure 3c. A slight increase of the size follows the pH increases and improves the formation of the Narcissus-like nanostructure. Concerning the nucleation stage, growth proceeds by nucleation of crystallites, then forming nanostructure grains which coalesce to cover the entire substrate surface and show a densely nanostructured film. Increasing the pH of the deposition bath increased the chance of the monomers gathering and forming the cone-like (leaf) shapes, and eventually, nanostructures were formed [26,42–44].

The same effect of time and temperature on the formation of ZnS Narcissus-like nanostructures can be seen clearly in Figures S2 and S3, respectively. The formation of nanostructures began after only 5 min of deposition, at which ZnS leaves appeared in the pre-formation stage with an average size of 200 nm (Figure S2a). When the deposition time reached 10 min, the Narcissus-like nanostructures had clearly emerged, as shown in Figure S2b. Further increase in the deposition time further enhanced the formation of ZnS nanostructures Figure S2c,d. With prolonged deposition, the Narcissus-like nanostructures also started to agglomerate and form more dense and larger size cone-like structures with an average size of more than 450 nm (Figure S2d).

Similarly, the formed structure is a cluster of leaf-like shapes distributed within the nanoscale regime with an average size of 220 nm in length with only $45\text{ }^\circ\text{C}$ (Figure S3a). Increasing deposition temperature to reach $65\text{ }^\circ\text{C}$, the Narcissus-like nanostructures with about 270 nm leaf size were formed (Figure S3b). This could be attributed to the effect of Ostwald ripening because larger particles are more energetically stable than smaller particles. Oriented attachment occurs because the aggregation decreases the interphase boundary and the total (surface) energy of the system [45]. Careful control of the deposition bath parameters can produce very homogeneous and regular ZnS Narcissus-like nanostructured thin films (Figure S4).

To investigate the optical properties of the prepared ZnS nanostructured thin films, the transmission measurements were conducted over a wide spectral range from 300 to 1100 nm. Figure S4 shows the variation of ZnS nanostructured thin-film transmission with different deposition parameters. The transmittance of the films inversely changed with the increase of the deposition parameters. For example, increasing the pH of the

solution forms more OH^- ions in the solution, which tend to be readily combined with zinc without leaving enough zinc on the substrate for ZnS growth [46,47]. The films were prepared at $T_d = 65^\circ\text{C}$, $t = 10$ min, Zn-conc. = 0.2 M, Tu-conc. = 0.2 M. Additionally, an increase in the bath temperature caused an increase in the particle kinetics in the solution that led to the formation of new ZnS grains which filled up the voids in the thin layer of the ZnS that eventually appeared to have more thickness and less transmittance [48]. Additionally, increasing Zn^{2+} ion concentration causes further aggregation of thicker and low transmittance nanostructured thin films [49].

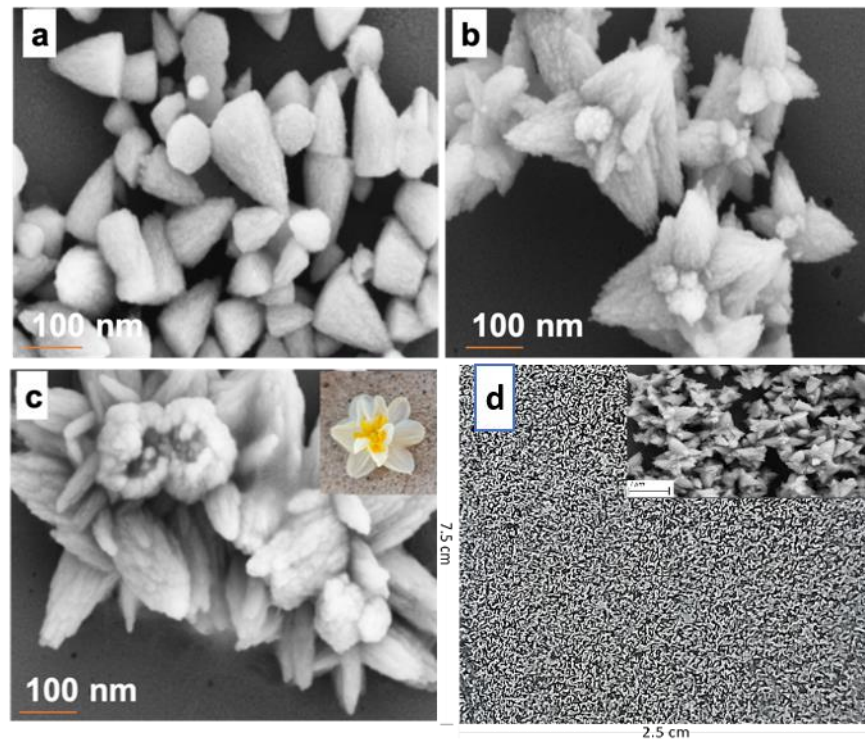


Figure 3. FESEM images formation of ZnS Nanostructure with different pH: (a) 9.5, (b) 10, and (c) 10.5. The inset of c is a real photo of the Narcissus flower. The films were prepared at $T_d = 65^\circ\text{C}$, $t = 10$ min. Zn conc. = 0.2 M, Tu-conc. = 0.2 M. (d) Magnified digital camera photo showing the homogeneous and regular ZnS Narcissus-like nanostructured thin film on glass substrate when deposition temperature was 65°C , pH 10, Zn and Tu-conc. = 0.2 M for 10 min. The inset is the FESEM image of the ZnS Narcissus-like nanostructure distribution on the substrate (with a scale of $1\ \mu$).

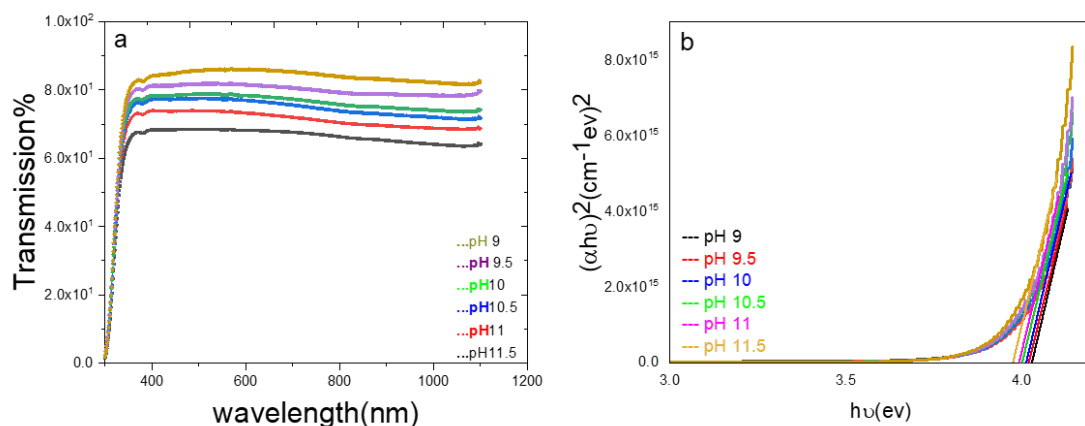


Figure 4. (a) The transmittance of ZnS thin films variation with different deposition pH (b) the E_g of ZnS thin at different pH levels. Other parameters were fixed at $T = 65^\circ\text{C}$, $t_d = 10$ min, Zn conc = 0.2 M, Tu- conc = 0.2 M.

From the transmission curves of the prepared ZnS Narcissus-like nanostructured thin films, the E_g was calculated from the plot of photon energy ($h\nu$) against the square of the product of absorption coefficients in photon energy $(\alpha h\nu)^2$ with different deposition parameters (Figure 4 and Table 1). The detailed E_g calculation with different deposition parameters can be seen in Figures S4 and S5.

Table 1. The variation of E_g with different deposition parameters.

Time(minutes)	5	10	20	30	40	50	60
E_g (eV)	4	3.995	3.99	3.98	3.97	3.94	3.92
pH	9	9.5	10	10.5	11	11.5	-
E_g (eV)	4.04	4.02	4.01	4	3.99	3.97	-
Temperature (°C)	40	45	55	65	75	-	-
E_g (eV)	4.06	4.04	4.02	4.01	3.99	-	-
Zn (CH ₃ COO) ₂ (M)	0.05	0.1	0.15	0.20	0.25	0.3	-
E_g (eV)	4.03	4.016	3.997	3.984	3.978	3.958	-
SC(NH ₂) ₂ (M)	0.05	0.1	0.15	0.20	0.25	0.3	-
E_g (eV)	4.03	4.02	4.01	4	3.995	3.990	-

From Figure S5 and Table 1, it can be concluded that the E_g of the deposited thin films reduced with the increase of the deposition parameters. The E_g values reduced from 4.04 eV to 3.97 eV after 60 min of deposition (Figure S5a). This is due to the increase in the film thickness and enlargement in the grain size of formed ZnS nanostructures as the deposition continuing (Figure S2, FESEM images). This reduced the film's transmission which in turn caused the reduction in the tangent of the absorption and, as a consequence, the E_g values were increased. The value of the E_g of the film that deposited for 60 min is comparable to the one that is recorded for the ZnS bulk E_g (3.79 eV) [50–52], while the values of the E_g of the ZnS Narcissus-like nanostructured thin film prepared at 10 min are higher, which can be attributed to the Quantum effect of the resultant structure within the film.

The variation of pH affected the E_g values of the deposited films: the highest value of about 4.04 eV for pH = 9 was recorded. This value reduced to about 3.97 eV with increasing the pH value to 11.5 which is higher than the ZnS bulk band gap (Figure 4b). Within the same deposition time (10 min, Figure S5f) a thinner film with a lower growth rate had a lower absorbance, thereby lower E_g and vice versa. Similarly, the same effect can be seen with the change in the bath temperature of the deposition (Figure S5c) and Table 1. With the rise in the bath temperature, the chemical reaction is accelerated, and therefore, the formation of ZnS nanostructures increased to produce a thicker film with a lower transmission. The effect of Zn concentration on the values of the E_g of the prepared thin films was more significant compared to the effect of Tu- concentration. The E_g decreased from 4.03 to 3.958 eV when the concentration of Zn raised from 0.05 to 0.3 M (Figure S5d). However, a small decrease in the energy bandgap of 4.03 eV to 3.99 eV was observed with the raise of Tu concentration (Figure S5e). This decrease in the E_g can be related to the reduction in the values of the S ions in the solution [53].

4. Conclusions

By using the CBD technique, ZnS Narcissus-like nanostructured thin films have been successfully deposited onto commercial glass substrates depending on different deposition parameters. The deposition parameters have a clear and direct effect on the morphology, structure, and energy bandgap of the prepared ZnS nanostructured thin films. Within the UV-VIS region, the optical characterization gives us a clear indication that enhancing ZnS thin films' E_g could extend their uses in a wide range of potential applications such as photovoltaic, detectors, and gas sensors.

Supplementary Materials: The following are available online at <https://www.mdpi.com/article/10.3390/coatings11091131/s1>, Figure S1. Schematic representation of the CBD system; Table S1. CBD

different deposition parameters. At each deposition, one of the parameters was changed and all others were fixed to get the optimized condition; Figure S2. FESEM images of ZnS Narcissus-Like Nanostructure growth with variation in deposition time (a) 5 min, (b) 10 min, (c) 30 min, (d) 60 min. The films Prepared at $T_d = 65$ C, Ph = 10, Zn conc. = 0.2 M, Tu conc. = 0.2 M; Figure S3. FESEM images of ZnS thin film formed with the different deposition temperature. (a) 45 °C, (b) 65 °C. The films Prepared at pH = 10, t = 10 mintes. Zn conc. = 0.2 M, Tu conc. = 0.2 M; Figure S4. Optical transmission spectra of ZnS thin films deposited at various (a) Times (b) pH (c) Temperatures (d) Zinc acetate concentration (e) Thiourea concentration; Figure S5. The optical energy gap of ZnS thin films deposited at various (a) Times (b) pH (c) Temperatures (d) Zinc acetate concentration (e) Thiourea concentration.

Author Contributions: Conceptualization, M.H.K., R.Y.M. and M.A.I.; data curation, M.H.K. and M.A.I.; formal analysis, R.Y.M. and M.A.I.; funding acquisition, M.H.K.; investigation, M.H.K., R.Y.M., and M.A.I.; methodology, M.H.K. and R.Y.M.; project administration, R.Y.M. and M.A.I.; resources, M.H.K.; software, M.H.K.; supervision, R.Y.M. and M.A.I.; validation, M.A.I.; visualization, R.Y.M. and M.A.I.; writing—original draft, M.H.K.; writing—review and editing, M.A.I. All authors have read and agreed to the published version of the manuscript.

Funding: This work was sponsored by the Department of Physics, College of Science, University of Duhok. This research received no external funding.

Institutional Review Board Statement: Not applicable.

Informed Consent Statement: Not applicable.

Data Availability Statement: Not applicable.

Acknowledgments: The authors would like to acknowledge Khider R. Khider for his kind effort for improving the quality of the paper.

Conflicts of Interest: The authors declare no conflict of interest.

References

1. Choudapur, V.; Bennal, A.; Raju, A. Influence of pH on optoelectronic properties of zinc sulphide thin films prepared using hydrothermal and spin coating method. *Mater. Res. Express* **2018**, *5*, 045201. [[CrossRef](#)]
2. Goudarzi, A.; Namghi, A.D.; Ha, C.-S. Fabrication and characterization of nano-structured ZnS thin films as the buffer layers in solar cells. *RSC Adv.* **2014**, *4*, 59764–59771. [[CrossRef](#)]
3. Long, F.; Wang, W.-M.; Cui, Z.-k.; Fan, L.-Z.; Zou, Z.-g.; Jia, T.-k. An improved method for chemical bath deposition of ZnS thin films. *Chem. Phys. Lett.* **2008**, *462*, 84–87. [[CrossRef](#)]
4. Li, Y. Photoluminescent Zinc Sulfide Optical Ceramics. Master's Thesis, New York State College of Ceramics at Alfred University, Alfred, NY, USA, 2015.
5. La Porta, F.A.; Andrés, J.; Li, M.S.; Sambrano, J.R.; Varela, J.A.; Longo, E. Zinc blende versus wurtzite ZnS nanoparticles: Control of the phase and optical properties by tetrabutylammonium hydroxide. *Phys. Chem. Chem. Phys.* **2014**, *16*, 20127–20137. [[CrossRef](#)]
6. Jiang, Y.; Zhang, W.J.; Jie, J.S.; Meng, X.M.; Zapien, J.A.; Lee, S.T. Homoepitaxial growth and lasing properties of ZnS nanowire and nanoribbon arrays. *Adv. Mater.* **2006**, *18*, 1527–1532. [[CrossRef](#)]
7. Fang, X.; Bando, Y.; Liao, M.; Zhai, T.; Gautam, U.K.; Li, L.; Koide, Y.; Golberg, D. An efficient way to assemble ZnS nanobelts as ultraviolet-light sensors with enhanced photocurrent and stability. *Adv. Funct. Mater.* **2010**, *20*, 500–508. [[CrossRef](#)]
8. Li, H.; Shih, W.Y.; Shih, W.-H. Non-heavy-metal ZnS quantum dots with bright blue photoluminescence by a one-step aqueous synthesis. *Nanotechnology* **2007**, *18*, 205604. [[CrossRef](#)]
9. Farhangfar, S.; Yang, R.; Pelletier, M.; Nielsch, K. Atomic layer deposition of ZnS nanotubes. *Nanotechnology* **2009**, *20*, 325602. [[CrossRef](#)]
10. Zhu, Y.-C.; Bando, Y.; Xue, D.-F.; Golberg, D. Nanocable-aligned ZnS tetrapod nanocrystals. *J. Am. Chem. Soc.* **2003**, *125*, 16196–16197. [[CrossRef](#)]
11. Gilbert, B.; Frazer, B.; Zhang, H.; Huang, F.; Banfield, J.; Haskel, D.; Lang, J.; Srajer, G.; De Stasio, G. X-ray absorption spectroscopy of the cubic and hexagonal polytypes of zinc sulfide. *Phys. Rev. B* **2002**, *66*, 245205. [[CrossRef](#)]
12. Shin, S.W.; Kang, S.R.; Gurav, K.; Yun, J.H.; Moon, J.-H.; Lee, J.Y.; Kim, J.H. A study on the improved growth rate and morphology of chemically deposited ZnS thin film buffer layer for thin film solar cells in acidic medium. *Sol. Energy* **2011**, *85*, 2903–2911. [[CrossRef](#)]
13. Haque, F.; Khan, N.; Rahman, K.; Islam, M.; Alam, M.; Sopian, K.; Amin, N. Prospects of zinc sulphide as an alternative buffer layer for CZTS solar cells from numerical analysis. In Proceedings of the 8th International Conference on Electrical and Computer Engineering, Dhaka, Bangladesh, 20–22 December 2014; pp. 504–507.
14. Shen, F.; Que, W.; Yin, X.; Huang, Y.; Jia, Q. A facile method to synthesize high-quality ZnS (Se) quantum dots for photoluminescence. *J. Alloys Compd.* **2011**, *509*, 9105–9110. [[CrossRef](#)]

15. Murai, H.; Abe, T.; Matsuda, J.; Sato, H.; Chiba, S.; Kashiwaba, Y. Improvement in the light emission characteristics of CdS: Cu/CdS diodes. *Appl. Surf. Sci.* **2005**, *244*, 351–354. [[CrossRef](#)]
16. Chen, Z.-G.; Zou, J.; Liu, G.; Lu, H.F.; Li, F.; Lu, G.Q.; Cheng, H.M. Silicon-induced oriented ZnS nanobelts for hydrogen sensitivity. *Nanotechnology* **2008**, *19*, 055710. [[CrossRef](#)] [[PubMed](#)]
17. Wang, X.; Xie, Z.; Huang, H.; Liu, Z.; Chen, D.; Shen, G. Gas sensors, thermistor and photodetector based on ZnS nanowires. *J. Mater. Chem.* **2012**, *22*, 6845–6850. [[CrossRef](#)]
18. Rajesh; Das, B.K.; Srinives, S.; Mulchandani, A. ZnS nanocrystals decorated single-walled carbon nanotube based chemiresistive label-free DNA sensor. *Appl. Phys. Lett.* **2011**, *98*, 013701. [[CrossRef](#)]
19. Elidrissi, B.; Addou, M.; Regragui, M.; Bougrine, A.; Kachouane, A.; Bernede, J. Structure, composition and optical properties of ZnS thin films prepared by spray pyrolysis. *Mater. Chem. Phys.* **2001**, *68*, 175–179. [[CrossRef](#)]
20. Bacha, K.B.; Timoumi, A.; Bitri, N.; Bouzouita, H. Structural, morphological and optical properties of sprayed ZnS thin films on various substrate natures. *Optik* **2015**, *126*, 3020–3024. [[CrossRef](#)]
21. Bosco, J.; Tajdar, F.; Atwater, H. Molecular beam epitaxy of n-type ZnS: A wide band gap emitter for heterojunction PV devices. In Proceedings of the 2012 38th IEEE Photovoltaic Specialists Conference, Austin, TX, USA, 3–8 June 2012; pp. 002513–002517.
22. Nicolau, Y. Solution deposition of thin solid compound films by a successive ionic-layer adsorption and reaction process. *Appl. Surf. Sci.* **1985**, *22*, 1061–1074. [[CrossRef](#)]
23. Yano, S.; Schroeder, R.; Ullrich, B.; Sakai, H. Absorption and photocurrent properties of thin ZnS films formed by pulsed-laser deposition on quartz. *Thin Solid Films.* **2003**, *423*, 273–276. [[CrossRef](#)]
24. Izi, M.; Heidari, G.; Khoie, S.M.; Najafi, J. Comparison of ZnS thin films fabricated by electrodeposition and spray pyrolysis methods. *Surf. Eng. Appl. Electrochem.* **2017**, *53*, 245–249. [[CrossRef](#)]
25. Tsai, P.-C.; Pai, I.; Shieh, H.-P.D. Two-stage chemical bath deposition for well-covered and stoichiometric ZnS thin films. In Proceedings of the 2012 38th IEEE Photovoltaic Specialists Conference, Austin, TX, USA, 3–8 June 2012; pp. 001992–001994.
26. Naseema, K.; Ribin, K.; Navya, N.; Prasanna, P. Thermal conversion of CBD grown ZnS thin films to ZnO. *Z. Nat. A* **2021**, *76*, 65–73.
27. Liu, Q.; Mao, G. Comparison of CdS and ZnS thin films prepared by chemical bath deposition. *Surf. Rev. Lett.* **2009**, *16*, 469–474. [[CrossRef](#)]
28. Liu, J.; Wei, A.; Zhao, Y. Effect of different complexing agents on the properties of chemical-bath-deposited ZnS thin films. *J. Alloys Compd.* **2014**, *588*, 228–234. [[CrossRef](#)]
29. Zein, R.; Alghoraibi, I. Influence of bath temperature and deposition time on topographical and optical properties of nanoparticles ZnS thin films synthesized by a chemical bath deposition method. *J. Nanomater.* **2019**, *2019*, 7541863. [[CrossRef](#)]
30. Hone, F.G.; Abza, T. Short review of factors affecting chemical bath deposition method for metal chalcogenide thin films. *Int. J. Thin Films Sci. Technol.* **2019**, *8*, 43–52.
31. Makuła, P.; Pacia, M.; Macyk, W. How to correctly determine the band gap energy of modified semiconductor photocatalysts based on UV-Vis spectra. *J. Phys. Chem. Lett.* **2018**, *9*, 6814–6817. [[CrossRef](#)] [[PubMed](#)]
32. Abdulla, M.M.; Hasan, N.H.; Mohammed, H.I.; Mohamed, G.H.; Al-Hamdani, K.A.; Abdulameer, A.F. Investigation of optical properties of the PbS/CdS thin films by thermal Evaporation. *J. Electron. Devices* **2012**, *12*, 761–766.
33. Mokili, B.; Froment, M.; Lincot, D. Chemical deposition of zinc hydroxosulfide thin films from zinc (II)-ammonia-thiourea solutions. *Le J. Phys. IV* **1995**, *5*, C3-261–C3-266. [[CrossRef](#)]
34. García-Valenzuela, J. Simple thiourea hydrolysis or intermediate complex mechanism? Taking up the formation of metal sulfides from metal–thiourea alkaline solutions. *Comments Inorg. Chem.* **2017**, *37*, 99–115. [[CrossRef](#)]
35. Bera, K.; Saha, S.; Jana, P.C. Temperature Dependent Synthesis of Zinc Sulfide Nanocrystal. *Orient. J. Chem.* **2018**, *34*, 1665.
36. Wei, A.; Liu, J.; Zhuang, M.; Zhao, Y. Preparation and characterization of ZnS thin films prepared by chemical bath deposition. *Mater. Sci. Semicond. Process.* **2013**, *16*, 1478–1484. [[CrossRef](#)]
37. Bolanle, Y.; Babatunde, R.; Adegboyo, O. Effects of deposition time of ZnS thin film on optical and morphological properties of ZnS deposited by chemical bath deposition method for photovoltaic application. *Phys. Mem. J. Theor. Appl. Phys.* **2019**, *1*, 38–45.
38. Iwashita, T.; Ando, S. Preparation and characterization of ZnS thin films by the chemical bath deposition method. *Thin Solid Films* **2012**, *520*, 7076–7082. [[CrossRef](#)]
39. Ke, H.; Duo, S.; Liu, T.; Sun, Q.; Ruan, C.; Fei, X.; Tan, J.; Zhan, S. Effect of temperature on structural and optical properties of ZnS thin films by chemical bath deposition without stirring the reaction bath. *Mater. Sci. Semicond. Process.* **2014**, *18*, 28–35. [[CrossRef](#)]
40. Lee, J.; Lee, S.; Cho, S.; Kim, S.; Park, I.Y.; Choi, Y.D. Role of growth parameters on structural and optical properties of ZnS nanocluster thin films grown by solution growth technique. *Mater. Chem. Phys.* **2003**, *77*, 254–260. [[CrossRef](#)]
41. Oliva, A.I.; Gonzalez-Chan, I.; Rejón, V.; Rojas, J.; Patiño, R.; Aguilar, D. Chemical bath method for ZnS thin films preparation. In Proceedings of the 2010 7th International Conference on Electrical Engineering Computing Science and Automatic Control, Tuxtla Gutierrez, Mexico, 8–10 September 2010; pp. 500–503.
42. Arun, S.; Kameswara, R.V.; Shrivastava, A.R.; Sanjay, U.; Deepika, J. Controlled Synthesis of Water Soluble Micrometer Sized Highly Luminescent Zinc Sulfide Flowers Using Green Chemistry Approach and Their Characterization. *ChemXpress* **2016**, *9*, 108.
43. Trindade, T.; de Jesus, J.D.P.; O'Brien, P. Preparation of zinc oxide and zinc sulfide powders by controlled precipitation from aqueous solution. *J. Mater. Chem.* **1994**, *4*, 1611–1617. [[CrossRef](#)]

44. Nasr, T.B.; Kamoun, N.; Guasch, C. Physical properties of ZnS thin films prepared by chemical bath deposition. *Appl. Surf. Sci.* **2008**, *254*, 5039–5043. [[CrossRef](#)]
45. AL-Diabat, A.M.; Ahmed, N.M.; Hashim, M.; Chahrour, K.M.; Bououdina, M. Effect of deposition temperature on structural and optical properties of chemically sprayed ZnS thin films. *Procedia Chem.* **2016**, *19*, 485–491. [[CrossRef](#)]
46. Nasr, T.B.; Kamoun, N.; Kanzari, M.; Bennaceur, R. Effect of pH on the properties of ZnS thin films grown by chemical bath deposition. *Thin Solid Films* **2006**, *500*, 4–8. [[CrossRef](#)]
47. Liu, W.-L.; Yang, C.-S.; Hsieh, S.-H.; Chen, W.-J.; Fern, C.-L. Effect of deposition variables on properties of CBD ZnS thin films prepared in chemical bath of ZnSO₄/SC (NH₂)₂/Na₃C₃H₅O₇/NH₄OH. *Appl. Surf. Sci.* **2013**, *264*, 213–218. [[CrossRef](#)]
48. Gumus, C.; Erkena, O.; Gunes, M.; Ozaslan, D. Effect of the deposition time on optical and electrical properties of semiconductor ZnS thin films prepared by chemical bath deposition. *Indian J. Pure Appl. Phys. IJPAP* **2017**, *55*, 471–477.
49. Haddad, H.; Chelouche, A.; Talantikite, D.; Merzouk, H.; Boudjouan, F.; Djouadi, D. Effects of deposition time in chemically deposited ZnS films in acidic solution. *Thin Solid Films* **2015**, *589*, 451–456. [[CrossRef](#)]
50. Borah, J.; Sarma, K. Optical and optoelectronic properties of ZnS nanostructured thin film. *Acta Phys. Pol. Ser. A Gen. Phys.* **2008**, *114*, 713. [[CrossRef](#)]
51. Yamaguchi, K.; Yoshida, T.; Lincot, D.; Minoura, H. Mechanistic study of chemical deposition of ZnS thin films from aqueous solutions containing zinc acetate and thioacetamide by comparison with homogeneous precipitation. *J. Phys. Chem. B* **2003**, *107*, 387–397. [[CrossRef](#)]
52. Gao, X.; Li, X.; Yu, W. Morphology and optical properties of amorphous ZnS films deposited by ultrasonic-assisted successive ionic layer adsorption and reaction method. *Thin Solid Films* **2004**, *468*, 43–47. [[CrossRef](#)]
53. Padmavathy, V.; Sankar, S.; Ponnuswamy, V. Influence of thiourea on the synthesis and characterization of chemically deposited nano structured zinc sulphide thin films. *J. Mater. Sci. Mater. Electron.* **2018**, *29*, 7739–7749. [[CrossRef](#)]